THE ASTROPHYSICAL JOURNAL, 369:111–120, 1991 March 1

A MERGER SCENARIO FOR NGC 7252: A TALE OF TWO TAILS

KIRK D. BORNE
Space Telescope Science Institute,[1] Homewood Campus, Baltimore, MD 21218
AND
DOUGLAS O. RICHSTONE
Department of Astronomy, University of Michigan, Ann Arbor, MI 48109
Received 1989 September 20; accepted 1990 August 17

ABSTRACT

Schweizer has proposed that NGC 7252 (Arp 226) recently formed from the merger of two disk galaxies and will ultimately relax into an elliptical galaxy. We have successfully simulated the suspected collision event with a gravitational interaction code, thereby reinforcing the merger hypothesis for the origin of this object. A careful selection of the disk and orbital model parameters lead to a good match to the present appearance and dynamics of this galaxy. Our best simulation relaxes into an object which morphologically and kinematically resembles a normal elliptical galaxy.

Subject headings: galaxies: individual (NGC 7252) — galaxies: interactions — galaxies: internal motions — galaxies: structure

1. INTRODUCTION

Toomre & Toomre (1972, hereafter TT) and Toomre (1977) identified several possible remnants of collisions between two disk galaxies. The peculiar galaxy NGC 7252 (also Arp 226) was one of their merger remnant candidates. This choice was based on the presence of two prominent plumes of material resembling the tidal tails seen in the simulated collisions of two disks described by TT. On the basis of its apparent collision-induced morphology and new measurements of the galaxy's complicated internal kinematics, Schweizer (1982, hereafter S82) further strengthened the arguments in favor of the disk + disk merger hypothesis for this galaxy. Figure 1 presents a reproduction of Schweizer's published blue photograph of the galaxy. Note the plumes extending to the east and northwest, and the complex structure near the center. Schweizer argues that the loops and filaments enveloping the main body of the galaxy are the remains of two colliding disks. In Figure 2 we present Schweizer's major and minor axis rotation profiles for the galaxy (where "major" and "minor" refer to the axes of a small gas disk of radius $\approx 8''$ surrounding the nucleus). Note the oscillating behavior of the major-axis profile, and the strong systematic motions along the minor axis $10''$–$20''$ from the center. Schweizer argues that these peculiar rotation properties along orthogonal axes in the galaxy may also have their origin in the two precollision rotating disks. It remains to demonstrate that some collection of collision parameters for two disks can indeed lead to a remnant whose properties match those of this unusual galaxy.

Using a "multiple three-body" stellar dynamical code developed by Borne (1982; 1984, hereafter Paper I; and 1988a, hereafter Paper II), we find a set of collision parameters for two rotating disks that reproduces the major morphological and dynamical features of NGC 7252 as described in S82. In the context of the particular simulation algorithm that we are using, our solution is confined to a limited range of model input parameters. The rich store of observational parameters strongly constrain the initial mass ratio of the disks, their relative orientation, the spatial and dynamical parameters of their initial orbit, the age of the remnant, and the total mass of the system. We therefore support Schweizer's conjecture concerning the origin of NGC 7252: the merger hypothesis is consistent with all of the observable properties of the system.

We presented the first draft of our solution in 1982 (Borne & Richstone 1982), and this has remained the most detailed example of a collision history for a putative merger remnant. Our greatest concern with our solution was the small size of the initial binary orbit; the observed properties of NGC 7252 could be matched only if the simulation of the colliding disks began at apocenter on a tightly bound elliptical trajectory. Barnes (1988) demonstrated that halos can tidally interact in a binary collision in such a way as to bring the luminous parts of the galaxies from an unbound trajectory onto a bound orbit in a very short time, before much damage to the luminous matter distribution has taken place. Hence, it is no longer a major concern that the initial orbit of our "luminous" disks is bound rather than unbound.

Schweizer (1982) went on to suggest that NGC 7252 is relaxing into an elliptical galaxy. By the time the collision-induced burst of star formation has subsided (in $\sim 10^9$ yr), he suggests that the galaxy should have the smoothness and radial luminosity profile of a typical elliptical. In fact, he showed that the current surface brightness profile, averaged over concentric rings, already closely follows the $r^{1/4}$ law that is generally ascribed to E galaxies. In support of Schweizer's suggestion, we find that our simulated remnant actually does relax to a smooth $r^{1/4}$ law.

In § 2 we describe the numerical model, while in § 3 we describe our search of the large parameter space of possible collisions for a particular solution. We quantitatively and graphically present our solution for NGC 7252 in § 4, where we also discuss its ramifications. Section 5 contains a summary and comments.

2. THE NUMERICAL MODEL

The calculations described in this paper use the multiple three-body algorithm (MTBA) described in Papers I and II.

[1] Operated by the Association of Universities for Research in Astronomy, Inc., for the National Aeronautics and Space Administration.

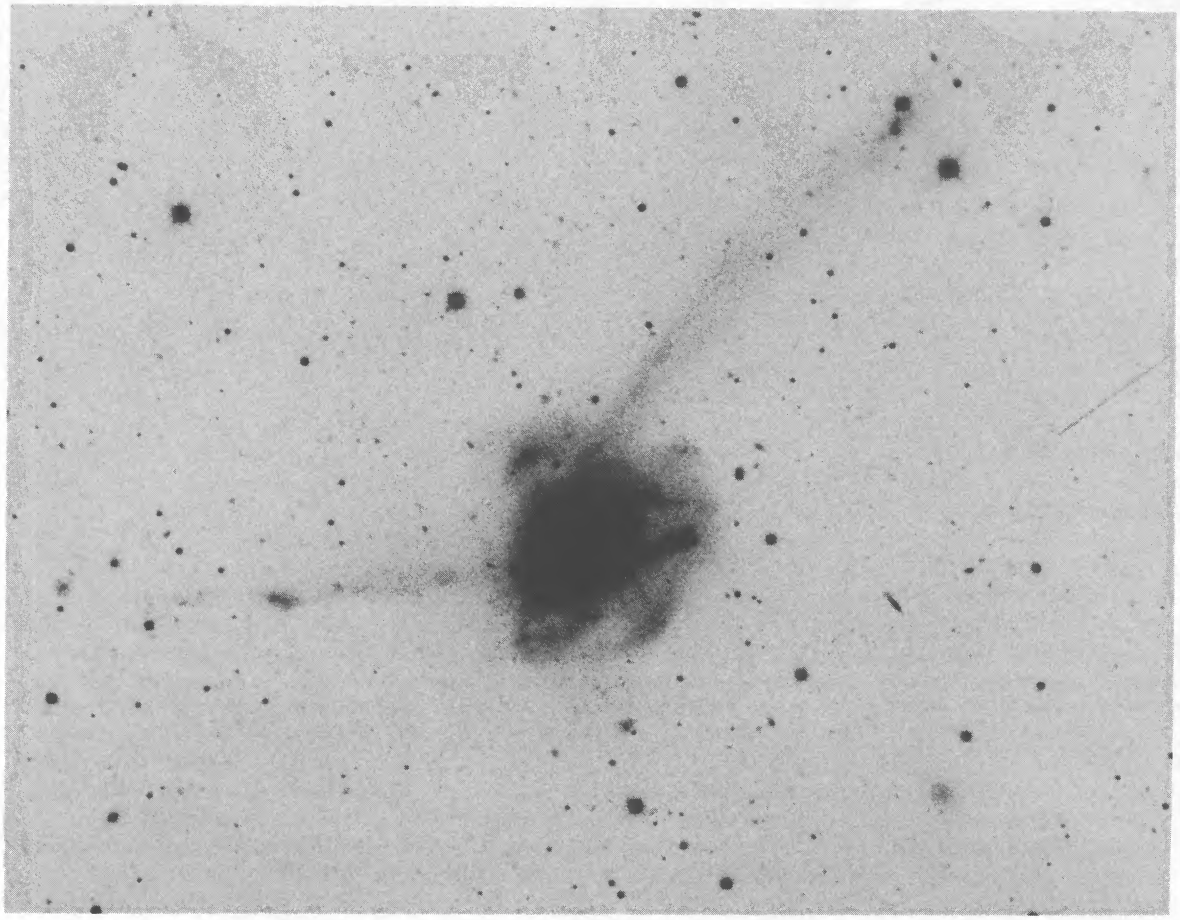

FIG. 1.—Schweizer's (1982) blue photograph of NGC 7252. North is up, and east is to the left. The diameter of the central burned-out region of the image is approximately 1′ (14 kpc h^{-1}).

This method has been used to model real interacting galaxies by Borne (1988b, hereafter Paper IV), Borne, Balcells, & Hoessel (1988, hereafter Paper V), and Balcells, Borne, & Hoessel (1989). The essential features of the "multiple three-body" stellar dynamical code follow.

In MTBA, each galaxy in a colliding pair is represented by a set of test particles. These test particles all respond to a pair of time-independent spherical potentials centered on the two galaxies, but the particles do not respond to gravitational forces from one another. The force on a given galaxy (i.e., on its center of mass) is simply the negative sum of all the forces that its potential field exerts on all of the test particles in the simulation. The forces of mutual interaction between the test particles and the centers of the two galaxies are thereby explicitly included. Because the center of potential for each galaxy thus interacts directly with all test particles, energy and angular momentum can be transferred from the bulk orbital motion of the galaxies into the individual test particles, many of which are lost from the system. This consequently allows for binary orbital evolution and, if so allowed by the physics of the interaction, orbital decay and the subsequent coalescence of the colliding pair through energy and angular momentum transfer. During this process, MTBA does not adjust the forms of the two galaxy potentials as their constituent particles are redistributed or lost. However, the initial particle configurations representing the model galaxies are subjected to a "proximity relaxation" phase, during which the phase-space distribution function of each galaxy (i.e., the combination of the mass, energy, and angular momentum distributions) is allowed to accommodate the proximity of the companion before any orbital evolution is allowed to proceed. Because MTBA requires only $2N$ force calculations at each time step (for an N-particle simulation), a large number of simulations can be investigated relatively quickly in order to identify the one set of model input parameters that best reproduces the observed state of a specific pair of interacting galaxies.

We use the potential of Paper I and the corresponding density distribution projected onto a plane. These functions were derived from a truncated Maxwellian velocity distribution. The spherical potential is given by

$$\phi(r) = k_1\left[\log_e(r^2 + a^2) - \frac{2}{3}r^2 + \frac{r^4}{10}\right] + k_2 \quad \text{for } r \le 1\,; \tag{1a}$$

$$\phi(r) = 1 - \frac{1}{r} \qquad \text{for } r > 1\,. \tag{1b}$$

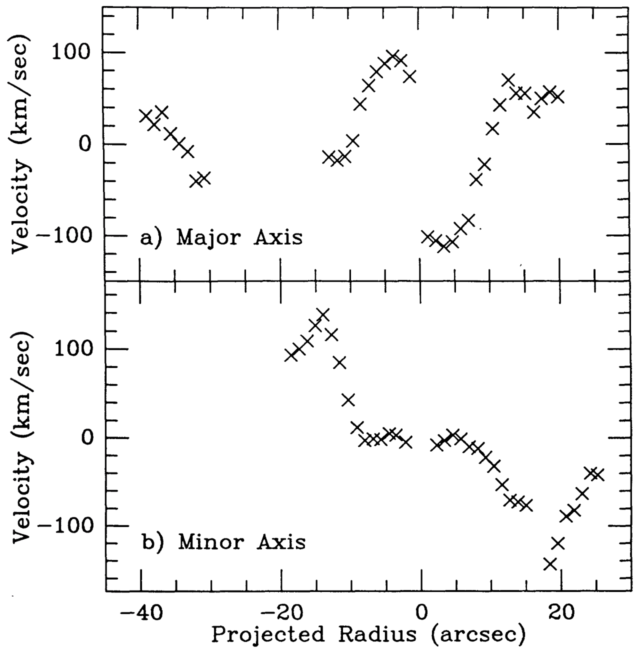

FIG. 2.—Schweizer's (1982) rotation profiles for NGC 7252 along the major and minor axes of the inner gas disk. (*a*) The major-axis profile was measured at position angle 115°, with negative projected radii to the southeast and positive projected radii to the northwest. (*b*) The minor-axis profile was measured at position angle 25°, with negative projected radii to the northeast and positive projected radii to the southwest.

Here, $k_1(\approx 0.94)$ and $k_2(\approx 0.53)$ depend on the model softening radius $a = 0.05$ (Paper I); we use units in which $G = M_d = R_d = 1$ for all simulations. Note that the form of the potential implies that $\rho(r) = 0$ for $r > 1$. The three-dimensional density law corresponding to the form of the potential at $r \leq 1$ is given by

$$\rho(r) = \frac{k_1}{2\pi}\left[\frac{r^2 + 3a^2}{(r^2 + a^2)^2} - 2 + r^2\right], \quad \text{for } r \leq 1 . \qquad (2)$$

This density distribution was projected onto a plane. The resultant profile follows closely the surface mass density of an exponential disk from about $r \approx 0.20R_d$ out to $r \approx 0.80R_d$, covering a range of ~ 5 disk scale lengths (scale length $\approx 0.12R_d$). A model disk is represented by a flat particle configuration comprising N_d particles, where $N_d = 1000$ in most of our preliminary simulations, and $N_d = 2000$ in the final best-fit simulation. Each disk galaxy is " built " with its own disk orientation and with all of its constituent particles initially placed on circular trajectories.

The technique we have used is clearly limited in three ways. First, we have ignored the halo component of each galaxy; these must surely have contributed to the prior evolution of the orbit, and may alter somewhat the appearance of the tails at large radii. Second, we have neglected the response of the disk *potentials* to the encounter; this would surely alter the appearance of the merger product, but we shall argue below that it does not affect our main conclusions. Finally, we are using a particle orbit code to model features that are seen in the gaseous component of the galaxy. This is legitimate only if the features we seek to model arise in gas that has only interacted gravitationally (and has not physically collided with gas clouds with very different velocities). This tactic must fail in the center, where a rapidly rotating gas disk has already formed, but must be substantially valid in the outer regions where very different velocities are seen in nearly the same projected positions. In our view, these limitations are offset by the economy of the technique used, which permits a large parameter study.

3. COLLISION PARAMETER SEARCH STRATEGY

A single collision can be characterized by (1) the mass ratio of the disks (one parameter), (2) their initial separation (one parameter), (3) their relative velocity vector in the orbital plane (two parameters), and (4) the angular momentum vectors of each disk (four parameters), for a total of eight parameters. In addition, the orientation of the line of sight to the observer relative to the orbit provides two more parameters. A full search of parameter space is clearly a most imposing task. Instead we have used physical intuition derived from our earlier simulations and those of TT to guide us to a satisfactory model. Because the strategy may be useful to future workers we sketch it below. Table 1 provides a detailed history of our search strategy, including orbital parameters, disk parameters, and remarks on each model's particular failure to reproduce key features of NGC 7252. Figures 3 through 6 provide an atlas of views of these simulations.

In an effort to reduce the complexity of the search somewhat, we initially made the *arbitrary* assumption that the two disk angular momentum vectors and the orbital angular momentum vector were coplanar. Interestingly enough, although this assumption allowed us to make rapid progress, it

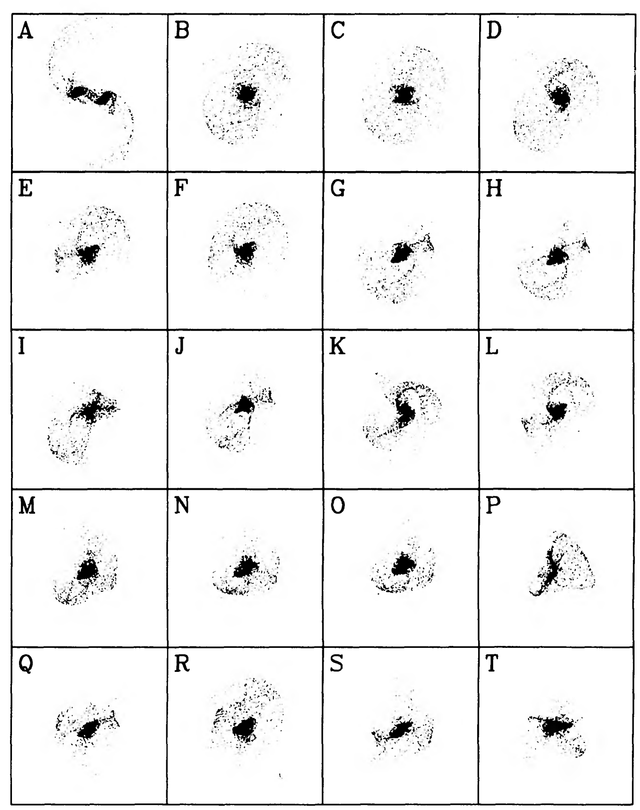

FIG. 3.—Top views of the first 20 simulations listed in Table 1; they are labeled according to the run no. given in the Table. All simulations are shown at the same model time (= 2.0). These are the same simulations as those that are shown from the side in Fig. 4. Nearly all of these simulations used 2000 particles.

TABLE 1

PARAMETERS FOR NGC 7252 MODEL SEARCH

Run no.[a]	M_2/M_1	Initial Separation[b]	Initial Velocity[b]	M_1 Rotation Axis[c]	M_2 Rotation Axis[c]	Reason for Model Failure
A	1.0	1.0	(0, 1.414)	(15, 90)	(30, 270)	No merger
B	1.0	1.0	(−0.5, 0.5)	(15, 90)	(30, 270)	Tail angle
C	1.0	1.0	(−0.5, 0.5)	(30, 270)	(30, 90)	Tail angle
D	0.6[d]	1.0	(−0.5, 0.4)	(30, 270)	(30, 90)	Tail angle
E	1.0	1.0	(−0.5, 0.5)	(45, 90)	(135, 90)	Tail angle and appearance
F	1.0	1.0	(−0.5, 0.5)	(30, 90)	(150, 90)	Tail angle and appearance
G	1.0	1.0	(−0.5, 0.5)	(120, 90)	(30, 90)	Tail angle and appearance
H	1.0	1.0	(−0.5, 0.5)	(120, 90)	(60, 90)	Major-axis rotation
I	0.5[d]	1.0	(−0.5, 0.4)	(120, 90)	(60, 90)	Multiple tails
J	0.8[d]	1.0	(−0.5, 0.4)	(120, 90)	(60, 90)	Major-axis rotation
K	0.5[d]	1.0	(−0.5, 0.4)	(60, 90)	(120, 90)	Tail angle and appearance
L	0.8[d]	1.0	(−0.5, 0.4)	(60, 90)	(120, 90)	Major-axis rotation
M	0.8[d]	1.0	(−0.5, 0.4)	(150, 90)	(90, 90)	Multiple tails
N	1.0	1.0	(−0.5, 0.4)	(150, 90)	(90, 90)	Multiple tails
O	1.0	1.0	(−0.4, 0.4)	(150, 90)	(90, 90)	Multiple tails
P	1.0	1.0	(−0.4, 0.4)	(90, 45)	(90, 135)	Tail appearance
Q	1.0	1.0	(−0.4, 0.4)	(120, 90)	(150, 90)	Tail appearance
R	1.0	1.0	(−0.4, 0.4)	(0, 0)	(150, 90)	Tail angle
S	1.0	1.0	(−0.4, 0.4)	(150, 90)	(120, 90)	Tail appearance
T	1.0	1.0	(−0.35, 0.2)	(150, 90)	(120, 90)	Minor-axis rotation
1	1.0	1.0	(−0.4, 0.4)	(120, 60)	(150, 60)	Multiple tails
2	1.0	1.0	(−0.4, 0.4)	(150, 90)	(120, 45)	Tail appearance
3	1.0	1.0	(−0.4, 0.4)	(150, 45)	(120, 90)	None. Best-fit model
4	1.0	1.0	(−0.4, 0.4)	(150, 135)	(120, 90)	Tail appearance
5	1.0	1.0	(−0.4, 0.4)	(150, 225)	(120, 90)	Tail angle
6	1.0	1.0	(−0.4, 0.4)	(150, 315)	(120, 90)	Tail appearance
7	1.0	1.0	(−0.4, 0.4)	(150, 150)	(120, 90)	Tail angle and appearance
8	1.0	1.0	(−0.4, 0.4)	(150, 120)	(120, 90)	Tail angle and appearance
9	1.0	1.0	(−0.4, 0.4)	(150, 60)	(120, 90)	Not as good as run no. 3
10	1.0	1.0	(−0.4, 0.4)	(150, 30)	(120, 90)	Not as good as run no. 3
11	1.0	1.0	(−0.4, 0.4)	(150, 45)	(120, 120)	Tail appearance
12	1.0	1.0	(−0.4, 0.4)	(150, 30)	(120, 75)	Multiple tails

[a] The "Run no." is coded according to the labels on the point plots shown in Figs. 3, 4, 5, and 6.

[b] Model units are defined in § 2. Physical equivalents of these units are presented in Table 2.

[c] Angles are spherical polar coordinates (θ, ϕ). The polar angle θ is measured from the $+z$ axis, which is parallel to the binary angular momentum vector, each binary orbit being confined to the xy plane. The azimuthal angle ϕ is measured from the $+x$ axis, which is parallel to the binary separation vector at time = 0.

[d] All simulations were run with $N_1 = N_2 = 1000$ except for those with non-unit mass ratio. Run D used $N_1 = 1500$, $N_2 = 900$; runs I and K used $N_1 = 1800$, $N_2 = 900$; and runs J, L, and M used $N_1 = 1200$, $N_2 = 960$. Here, N_i is the number of particles assigned to galaxy i.

failed when we attempted to match the minor axis rotation curve—so it was not possible to make any arbitrary assumptions about the original orbit.

3.1. *Tail Morphology*

Our initial prejudice (based on the presence of two tails) was that both disks were prograde with respect to the orbit. Then, the rough equality of length and luminous material in each tail constrains the mass ratio of the two disks to lie near unity. Although it subsequently developed that both disks must be more nearly retrograde, this result survived. The lack of curvature in the tails forced us to always position the observer near (within 20° of) the plane of each disk. Given these considerations, it was easy to find various collision parameters that produced the correct tail morphology. Run H, in Figure 4, was the first model to show this.

3.2. *Major Axis Rotation*

While the appearance of the tidal tails in NGC 7252 only weakly restricts the volume of parameter space containing possible collision solutions for this system, the oscillating major-axis rotation curve (Fig. 2*a*) strongly constrains the range of model input parameters. In particular, the possible orientations for the initial galaxies' internal spin axes relative to the orbital angular momentum vector are well-constrained. Because of this, many more test runs were required to match the kinematics of this galaxy than were required to match the appearance of its tidal tails. Run T, in Figure 4, was the first run to match both the tidal tails and the major axis rotation profiles. In particular, we found that if either of the two disks were rotating prograde (as we had initially assumed), then the resultant major-axis rotation profile of the remnant would have had a much greater amplitude and would have portrayed much more systematic rotation: strongly receding velocities on one side, strongly approaching on the other. This is simply the result of the strong tidal response of prograde stellar orbits in close encounters (TT; see also McGlynn & Borne 1990 and references therein).

The merger of a pair of retrograde-rotating disks results in a remnant with *opposite* spin contributions from the external and internal angular momenta. This results in a system with both receding and approaching velocities on the same side of the galaxy (as projected onto the plane of the sky), in accord with the observed rotation profiles in NGC 7252. Clearly, if

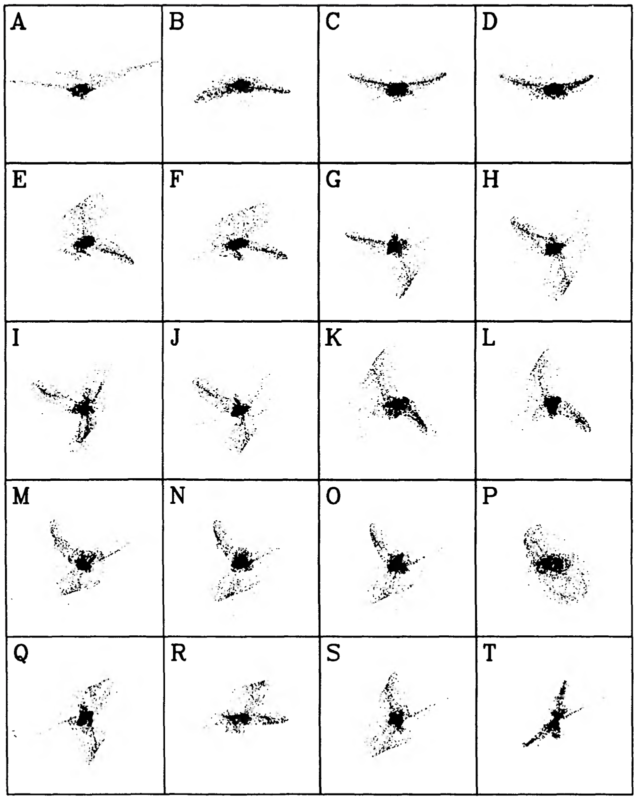

FIG. 4.—Side views of the first 20 simulations listed in Table 1; they are labeled according to the run no. given in the Table. All simulations are shown at the same model time (= 2.0). These are the same simulations as those that are shown from the top in Fig. 3. Note that several of these look very similar to NGC 7252. However, in no case are the model's rotation profiles similar to those observed.

these two oppositely rotating components are gaseous, then they cannot occupy the same location in space without substantial dissipation and disruption of the velocity flow. It is then necessary that the different parts of NGC 7252's rotation curve that are alternately approaching and receding correspond to spatially separate dynamical components that appear side-by-side in projection only (otherwise the oscillations would not be seen in the dynamics of the gas, *as they are*). Quantitatively, this restricts the range of angles that are allowed both for the disk spin vectors (which must be roughly retrograde) and for the viewing angle of the observer.

3.3. *Minor Axis Rotation*

Our single most difficult task was matching the observed minor-axis rotation profile while simultaneously matching both the appearance of the tidal tails and the observed major-axis rotation profile. At this point (run 2) we were forced to abandon our arbitrary assumption that the three angular momentum vectors were coplanar. The mechanics which produce this rotation curve are discussed in § 4.4.

4. THE BEST-FIT SIMULATION

In this section we discuss our adopted physical solution for NGC 7252, and various "observational" properties of this model. Table 2 presents an itemized list of the corresponding model and physical parameters defining our solution.

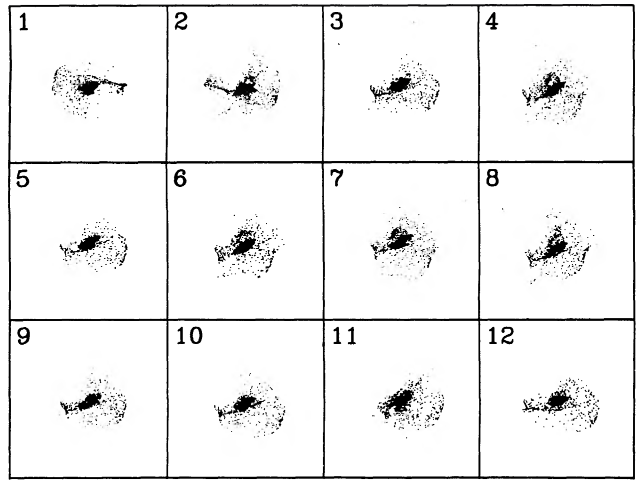

FIG. 5.—Top views of the last 12 simulations listed in Table 1; they are labeled according to the run no. given in the Table. All simulations are shown at the same model time (= 2.0). These are the same simulations as those that are shown from the side in Fig. 6. All of these simulations used 2000 particles.

4.1. *Binary Orbital Parameters*

As discussed in the previous section, the mass ratio of the pair of disk galaxies that formed NGC 7252 must be close to unity, being constrained by the similar lengths of the two tidal tails. We found that this value is correct to within a factor of 2 by running a series of test simulations (not all of which are listed in Table 1, but see runs D and I through M in Fig. 4); as the mass ratio deviates more and more from unity, the strengths of the two tidal tails become more disparate. We used a mass ratio of one in our best-fit simulation.

We find that the orbit of the colliding pair is constrained by the age of the interaction, as indicated by the lengths and appearances of the tidal tails. A large orbit decays so slowly that the tidal tails will be very long and will have lost their sharpness by the time the two galaxies merge. The tails may

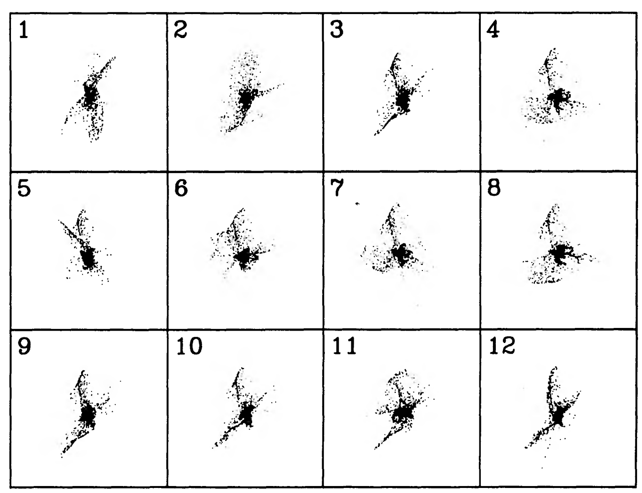

FIG. 6.—Side views of the last 12 simulations listed in Table 1; they are labeled according to the run no. given in the Table. All simulations are shown at the same model time (= 2.0). These are the same simulations as those that are shown from the top in Fig. 5. Though several of these look very similar to NGC 7252, only in one model (no. 3) did both the major- and minor-axis rotation profiles match the observations.

TABLE 2

Adopted Physical Parameters for NGC 7252

Parameter	Model Units	Physical Units
Heliocentric redshift[a]	...	4749 ± 3 km s^{-1}
Redshift relative to Local Group	...	4828 ± 3 km s^{-1}
Distance	...	48.3 Mpc h^{-1}
Total absolute B magnitude[b]	...	-20.63
Mass ratio of initial pair of galaxies	1.0	...
Extent of east tail from nucleus	1.5	$3'.8 \simeq 53$ kpc h^{-1}
Extent of NW tail from nucleus	1.5	$4'.7 \simeq 66$ kpc h^{-1}
Semiamplitude of major-axis "rotation"	1.2	105 km s^{-1}
Semiamplitude of minor-axis "rotation"	?	140 km s^{-1}
Mass of remnant[c]	2.0	$1.3\text{–}1.6 \times 10^{11}\ M_\odot\ h^{-1}$
M/L_B[c]	...	$5\text{–}6h\ M_\odot/L_\odot$
Age of interaction[d]	2.0	$8\text{–}10 \times 10^8$ yr h^{-1}
Settling time for "elliptical" remnant[d,e]	~ 5	$\sim 2 \times 10^9$ yr h^{-1}
Flattening of remnant	E4	...
V_{rot}/σ for remnant	0.4	...

[a] From S82.

[b] From S82, except that we use $H_0 = 100$ km s^{-1} Mpc^{-1}.

[c] Mass $\propto$ length $\times$ (speed)^2: the velocity scale is set by the semiamplitude of the major-axis rotation profile, whereas the lower limit on the length scale is set by the length of the east tail and the upper limit on the length scale is set by the length of the NW tail.

[d] Time $\propto$ length $\div$ speed: see note c above.

[e] Approximate time for stellar orbits in remnant to phase mix sufficiently to smooth out the most prominent features of the interaction (e.g., the tails and loops).

also become wrapped around the remnant galaxy during the long decay time, rendering their appearance significantly different from that observed. On the other hand, a small orbit would have decayed so early on in the universe that it requires a special explanation for the apparently young age of the currently observed remnant. Our best-fit simulation does in fact have a very small apocenter distance. However, this orbit corresponds only to the luminous components of the colliding disks. This tightly bound orbit may have evolved from the rapid orbital decay of the binary during the tidal interaction of the galaxies' massive dark halos (Barnes 1988). In our model units, the binary orbital parameters of the best simulation are $a = 0.544$ (semimajor axis), $e = 0.923$ (eccentricity), $R_{apo} = 1.0454$, and $V_{apo} = 0.383$. The derived translations from model to physical units are listed in Table 2.

4.2. *Model Galaxy Parameters*

The disk orientations for galaxies 1 and 2 are described by the orientations of their angular momentum vectors. In spherical polar coordinates, these are ($\theta_1 = 150°$, $\phi_1 = 50°$) and ($\theta_2 = 120°$, $\phi_2 = 95°$). The angle θ is the polar angle measured from the direction defined by orbital angular momentum vector and ϕ is the azimuthal angle measured counterclockwise in the orbital plane from apocenter. Note that this definition of ϕ differs by 5° from that used in Table 1; there the angle was measured from the $+x$ axis, the line connecting the galaxy centers at the beginning of each simulation. A schematic representation of the initial orientation of the two disks used in our best-fit simulation is shown in Figure 7. The binary orbit defines the xy plane, with galaxy 2 located on the $+x$ axis at time = 0. In Figure 7, the viewer is located in the direction ($\theta_{view} = 78°$, $\phi_{view} = -114°$), chosen simply to provide an instructive illustration of the relative orientations of the disks in our best-fit simulation. This direction contrasts with the viewing angle used in subsequent figures to produce the best match between the simulation and the observations of NGC 7252: ($\theta_{obs} = 75°$, $\phi_{obs} = 30°$); see § 4.3. Hence, in Figure 7, the observer is looking at the system *very roughly* back into the direction of an Earth-bound observer.

As described in § 3.2, the orientations of the two colliding disks were constrained by the major and minor axis rotation profiles published in S82. The various models outlined in Table 1 indicated to us that the range of uncertainty in these orientations is probably $\pm 15°$.

4.3. *Observer Orientation*

We find the best position to be in the direction of ($\theta_{obs} = 75°$, $\phi_{obs} = 30°$). This means that the plane of the binary orbit is tilted by 75° from the plane of the sky (i.e., the observer is only

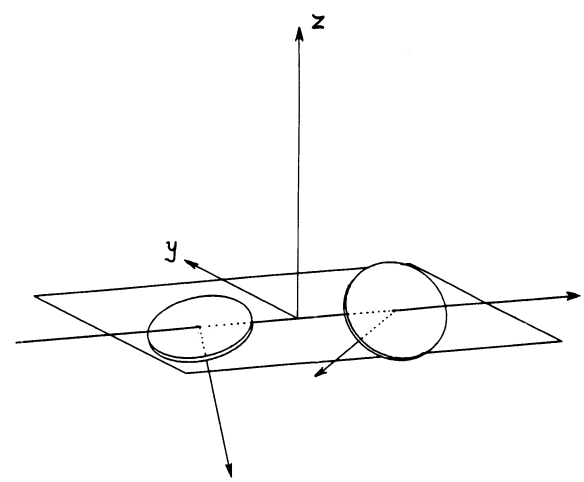

Fig. 7.—Schematic representation of the initial orientations of the two colliding disks *at apocenter* in the best-fit simulation of NGC 7252. The orbit of the pair lies in the xy plane, with galaxy 1 located on the $-x$ axis and galaxy 2 located on the $+x$ axis at time = 0. In normal spherical polar coordinates, the rotation axes of the disks are ($\theta_1 = 150°$, $\phi_1 = 50°$) and ($\theta_2 = 120°$, $\phi_2 = 95°$). Here the azimuthal angle ϕ is measured with respect to the separation vector at apocenter.

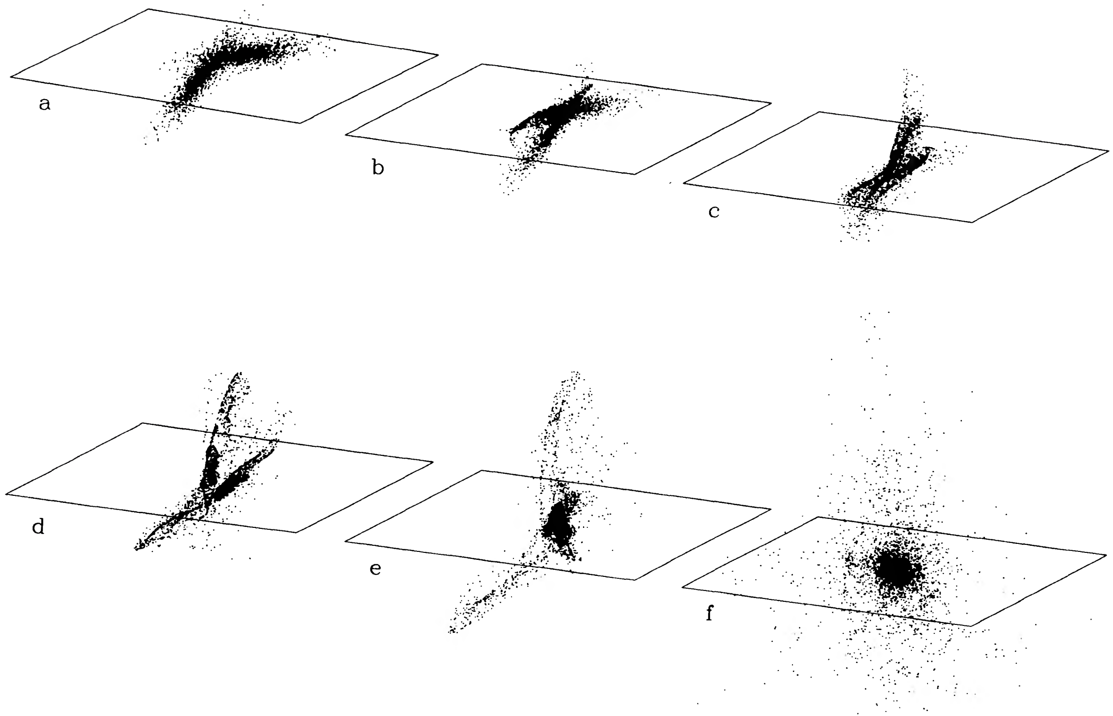

FIG. 8.—Time development of the best-fit simulated collision model for NGC 7252. Two rotating disks, with 2000 particles each, represent the colliding progenitors. Galaxy 1 is represented by the near-horizontal disk of particles and galaxy 2 by the near-vertical disk of particles which is initially (in Fig. 8*a*) to the left and in front of galaxy 1. The viewing angle for all of the plots shown here corresponds to a position ($\theta_{obs} = 75°$, $\phi_{obs} = 25°$) in normal spherical polar coordinates, where the orbit is constrained to line in the xy plane and the galaxies are placed along the x axis at time = 0 (frame *a*). The snapshots in frames (*b*), (*c*), (*d*), (*e*), and (*f*) were taken at model times 0.50, 1.00, 1.50, 2.00, and 5.50, respectively. Frame (*e*) corresponds to the time when we find the best match between the model and all of the observations of NGC 7252. It is at this point that the galaxies have merged into a single galaxy. Note the lengths of the tidal tails, the curvature of the upper tail, the straight lower tail, and the loops crossing the center of the galaxy. These accurately emulate the observed morphology of NGC 7252 (Fig. 1). Frame (*f*) shows how the remnant has settled down and begun to look a lot like a normal elliptical; the tidal tails are becoming less distinguishable, becoming part of the galaxy's faint outer envelope.

15° above the original binary orbital plane). As meausred along that collision trajectory, the observer is 30° beyond the apocenter position (i.e., 150° ahead of the original pericenter position).

4.4. *The Collision Solution*

In Figure 8 we show the time development of our best-fit collision simulation, as seen from the viewing angle specified above, which was required to match all of the observations of NGC 7252 reported in S82. Each galaxy is represented by 2000 particles. Galaxy 2 is initially in the foreground (Fig. 8*a*) and is moving left to right. Each of the first five frames in Figure 8 are separated by a little over one internal crossing time. The first five frames therefore span a duration of almost five crossing times. The last two frames in the figure are themselves separated by nearly 10 crossing times. The final particle configuration (Fig. 8*f*) shows how the system has settled down, becoming more and more symmetric in appearance; the tidal tails gradually lose their sharpness and ultimately their distinguishability.

Figure 8*e* presents our best-fit model snapshot of the NGC 7252 system; compare this with Figure 1 (from S82). Note the length and curvature of the two tidal tails, and note the various loops and filaments near the center of the remnant galaxy. The observed features (Fig. 1) are well-reproduced in the simulation (Fig. 8*e*).

The major and minor axis velocity profiles of our model remnant are shown in Figures 9*b* and 9*d*, alongside of which are small contour maps (Figs. 9*a* and 9*c*) showing the placement of the "spectroscopic slit" in each case. Compare these rotation profiles with those shown in Figure 2 (from S82). In particular, note the oscillating behavior of the major-axis profile (Fig. 9*b*), and the nonzero minor-axis rotation off the nucleus (Fig. 9*d*). Such a multiple-component velocity field, where the direction of rotation is highly spatially variable, is indicative of a lack of dissipation in these tidal features. On the other hand, the observed minor-axis rotation profile (Fig. 2*b*) is flat at the center of the galaxy (where S82 reports seeing a small gas disk), whereas our model's minor-axis rotation profile (Fig. 9*d*) is not flat. This difference in fact represents evidence for dissipation in the gaseous component at the center of the real galaxy, which is not modeled in our stellar dynamical simulations (see § 4.5).

The few differences that do exist between our model's major-axis rotation profile (Fig. 9*b*) and that observed by S82 (Fig. 2*a*) include the specific radial positions at which the velocities reach a local maximum, the precise amplitudes of the velocity variations, and the steepness of the velocity gradient around the origin. The detailed matching of these features depends on the finer details of our initial galaxy model (e.g., its rotation and mass distribution) and on the true orbital decay path of the two disks. We therefore cannot expect a perfect match between theory and observation in the context of the current

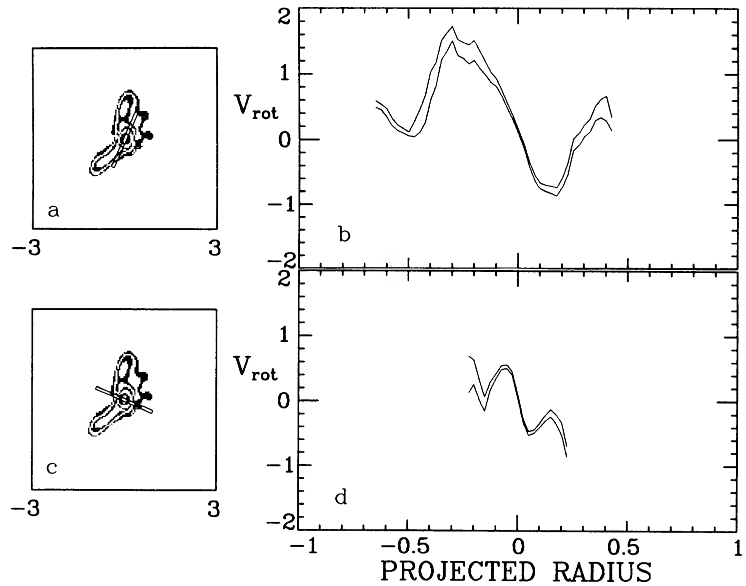

FIG. 9.—Rotation velocity profiles as measured in the simulated merger remnant (Fig. 8*e*) along the major (*top*) and minor (*bottom*) axis directions defined in S82. The slit orientations are shown in the accompanying contour maps alongside each rotation profile. In profile (*b*), negative projected radii correspond to the bottom half of the slit show in map (*a*); in profile (*d*), negative projected radii correspond to the left half of the slit shown in map (*c*). Each rotation profile is represented by two curves, corresponding to the mean velocity ± one standard deviation at each position along the slit (see Paper II). Note the oscillating behavior of the major-axis curve (*b*) and how it emulates the variations seen in Fig. 2*a*. Also note the nonzero rotation rate along the minor axis (*d*), and how that is similar to what is seen at large radii in Fig. 2*b*; differences between the observed and simulated minor-axis profiles are discussed and rectified in §§ 4.4 to 4.5.

numerical model, but the degree to which the two curves are similar is sufficient to indicate that the adopted solution is quite reasonable.

Likewise, our model's minor-axis rotation profile (Fig. 9*d*) differs in understandable ways from that observed by S82 (Fig. 2*a*), as mentioned above. In addition to the lack of proper treatment of dissipation in the core of the remnant, our collision simulation uses too few particles to fully sample the minor-axis rotation profile out to radii as large as those studied by S82 where a strong nonzero component of rotation was detected (Fig. 2*b*). However, our minor-axis profile (Fig. 9*d*) does in fact show the correct behavior in having significant positive velocities at negative projected radii, and vice versa.

A full map of the best-fit model's velocity field is presented in Figure 10. In that figure, the size of the symbol is proportional to the magnitude of the velocity, and the type of symbol indicates its sign (+ indicates a velocity into the page, and × indicates a velocity out of the page). Note the high spatial variability of the velocity field in the central regions of the remnant, showing rapidly alternating positive and negative line-of-sight velocities, and also note the existence of high-velocity spots, similar to those reported in S82.

Taken together, the particle distribution (Fig. 8*e*) and the velocity map (Fig. 10) of our best-fit simulation provide the best explanation of the appearance of the major and minor axis rotation profiles. For each profile the spectroscopic slit passes across different pieces of the still rotating remains (tails and loops) of the initial galactic disks. For example, the minor axis rotation (Fig. 9*d*) can be seen in Figure 10 to be the result of the positive (receding) velocities just to the left of center and the negative (approaching) velocities just to the right of center. We can see in fact that the upper tail in Figures 8*e* and 10 passes to the left of the remnant's center and then loops around to the bottom of the galaxy, and we can see that the lower left tail passes to the right of the remnant's center and then loops around to the top; these together conspire to give the observed minor-axis rotation profile. A similar analysis holds for the major-axis velocities.

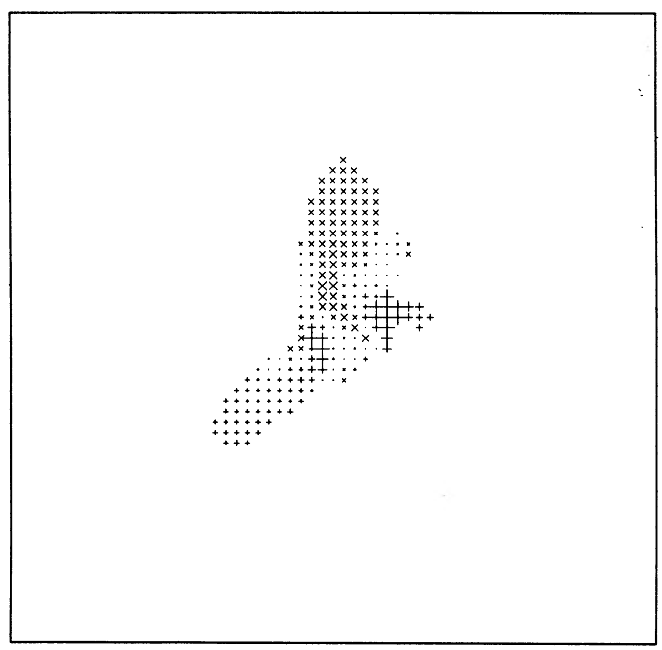

FIG. 10.—Map of of the velocity field in the merger remnant at the current epoch (Fig. 8*e*). Symbols are described in the text (§ 4.4). Note the high spatial variability of the velocity field near the center and the occasional high-velocity peaks, similar to those reported in S82. One can trace the correspondence between the tidal tails and loops in Fig. 8*e* with the velocity field shown here. In particular, one can identify the kinematic traces and signatures of the initial disk rotations.

The upper tidal tail in Figures 8*e* and 10 is the remnant of the galaxy 2 disk (the one that *appears* at a 45° angle in the lower half of Fig. 8*a*). That disk was rotating such that the upper part was coming toward us, and the lower part was receding. Those motions are preserved in that disk's tidal debris: in Figure 10 we see strong approaching velocities in the upper tail, strong recession velocities to the left of center, and equally strong recession velocities to the right of center where it curves back around the galaxy.

The lower left tidal tail in Figures 8*e* and 10 originates just above the center of the galaxy in a small loop that comes across the center and to the lower right of center before finally extending more fully to the lower left. These are the remains of the galaxy 1 disk (appearing almost horizontal in the upper portion of Fig. 8*a*). The rotation vector of that disk was pointing down, so that the right side was approaching us and left side was receding. The initial rotation is still evident in that disk's tidal debris: in Figure 10 we see approaching velocities at the center of the galaxy and just to the right of center, and we see recession velocities in the lower left tail. The latter are not very strong, indicating that the motion of this tail is mostly transverse to the line of sight.

The interpretations given above can be tested (as can our full velocity map) with additional spectroscopic work on this galaxy. In fact, S82's velocity measurements at the ends of the tidal tails and just to the west of the galaxy center are all consistent with the model velocities represented in Figure 10.

It is worth reemphasizing that the observed rotation velocity profiles were critical to isolating a unique collision model for the NGC 7252 system (see §§ 3.2–3.3 and also the arguments in Papers II, IV, and V). Such kinematic data strongly constrain the internal parameters of the colliding disks, particularly the relative orientations of their rotation axes with respect to the collision trajectory. Many different collision models starting off with very different disk orientations will result in a merger remnant having tidal tails similar to those observed in size, shape, and orientation. But very few of those models will have the correct major-axis rotation profile, and only an isolated range of the remaining models will have the correct minor-axis rotation profile.

4.5. *Dissipation*

The loops and filaments seen encompassing the central region of NGC 7252 in Figure 1 are the physical remains of the two initial disks. In some cases, one can follow the outer tidal tails into this region and actually identify some of the loops as continuations of those tails wrapping around the galaxy (see § 4.4). The observed oscillations in the major- and minor-axis rotation profiles are simply the result of the spectroscopic slit crossing these various spatially distinct dynamical components (§ 4.4). Except at the very center of the galaxy, there has been no physical contact between these loops of gas; the dynamical components appear to overlap only in projection. This property of the model is crucial for the validity of our procedure. Had gas clouds from these two components collided we would not have been justified in studying this encounter with a pure gravitational dynamics code.

At the center of NGC 7252 there is dissipation, as the orbits of the gas clouds in the two disks have crossed. There are two manifestations of the dissipative processes at work there: (1) the gas forms a rapidly rotating disk (as described in S82); and (2) all motions transverse to the disk plane are damped, erasing any systematic rotation of the gas along the minor axis. The latter operates only out to the distance where the gas clouds collide (i.e., where dissipation is active). Beyond that radius, the distinct dynamical signatures of the two initial gas disks are not erased, leading to the strongly nonzero minor-axis rotation velocities measured at projected radii of a few kpc from the galaxy center. Because our models do not include any form of gas dynamics or dissipation, a rotating disk does not form at the center of our model remnant and the minor axis rotation is not damped at small radii. We believe this explains the difference between the small-radius behavior of our minor-axis rotation profile (Fig. 9*d*; nonzero velocity gradient) and that of S82 (Fig. 2*b*; extended region of zero rotation).

4.6. *The Merger Remnant*

Figure 8*f* shows the model remnant as it appears while settling down, approximately 1.5×10^9 yr after the current epoch. In roughly the next 10^9 yr, the model remnant will assume a very symmetric appearance, with E4 flattening and a radial surface brightness profile indistinguishable from a de Vaucouleurs $r^{1/4}$ law. The model also settles down dynamically on this same time scale. Figure 11 presents the initial and future line-of-sight velocity distribution for all of the particles in our best-fit simulation of NGC 7252: the upper panel shows the structure appropriate for the superposition of the two rotating disks at time = 0, and the lower panel shows the distribution at model time = 8. (Recall that model time = 2 corresponds to the current epoch, and that, from Table 2, one unit of model time corresponds to 4–5 $\times 10^8$ yr.) The velocity distribution shown in the lower panel of Figure 11 is very symmetric, even somewhat Gaussian-like, indicating that a very high degree of

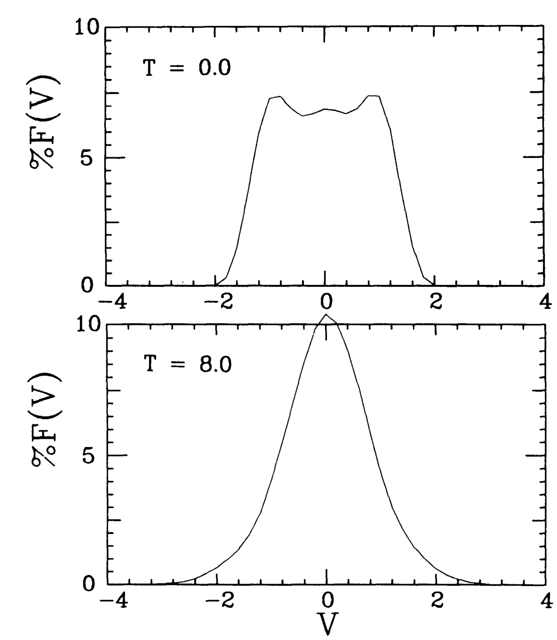

FIG. 11.—Line-of-sight velocity distribution functions for the 4000 particles in the best-fit simulation, showing the fractional percentage of particles in the different velocity bins at two different model times. Model time = 0 corresponds to the configuration shown in Fig. 8*a*, and model time = 8 corresponds to the settled, relaxed merger remnant nearly 3×10^9 yr from now. Note the signatures of the two rotating disks in the initial distribution, and note the smooth, symmetric shape of the final distribution. The latter indicates that the remnant galaxy is in a dynamically relaxed state, presumably resulting from the large degree to which the system has been phase-mixed by violent relaxation during the merger event.

relaxation and phase-mixing has occurred in the remnant by this time. The rotation rate in our model remnant (at model time = 5.5; Fig. 8*f*) corresponds to $V_{\rm rot}/\sigma \approx 0.4$, which is appropriate for a bright E4 galaxy (see Illingworth 1981).

The large rotational amplitude in our simulation near the center must correspond to the rapidly rotating gas disk seen by Schweizer. The presence of such rapid rotation does not appear to be a problem for simulators, nor for the identification of the object as a nascent elliptical galaxy, as various authors have noted the presence of rapidly rotating distinct dynamical subsystems in elliptical galaxies or bulges (see Franx & Illingworth 1988; Jedrzejewski & Schechter 1988; and Bender 1988).

5. SUMMARY

TT and S82 have suggested that NGC 7252 formed from the merger of a pair of disk galaxies. Our goal was to simulate the collision of two galaxies whose merger remnant had a structural appearance and velocity field that matched those observed for NGC 7252. We succeeded in this by finding a set of initial orbital and rotation parameters for two disks that evolved (through tidal processes during the encounter) into an NGC 7252 look-alike (compare Fig. 1 with Fig. 8*e*). We had no problem finding a simulation whose merger remnant included two nearly straight tidal tails at the proper relative position angle. This was accomplished through the careful selection of initial disk orientations and observer viewing angle. The initial trajectory, disk orientations, and mass ratio of the pair of "galaxies" were chosen so as to provide the best match between simulation and observed data. Somewhat more care was required to find a simulation whose major-axis rotation curve matched the oscillatory curve published in S82 (compare Fig. 2*a* with Fig. 9*b*). Our simulations indicate that such a curve results from the merger of two disks rotating in a nearly retrograde sense relative to their initial orbital angular velocity. Finally, after several additional simulations, we were able to match the minor-axis rotation profile of S82 (compare Fig. 2*b* with Fig. 9*d*). This was accomplished by judicious choice of the orientation of the three (nonplanar) angular momentum vectors.

TT and S82 not only proposed an origin for NGC 7252, but they also predicted its fate: it is likely to become a normal elliptical galaxy. We support that prediction. Our best-fit simulation was followed for about 10 dynamical times after the merger event in order to determine the fate of the merger remnant. After this period of relaxation and phase-mixing, the resulting remnant takes on a smoother, more symmetric appearance and has a luminosity profile consistent with the $r^{1/4}$ law. Its rotation rate is also consistent with that of a normal elliptical galaxy. With a ratio of maximum rotation velocity to central velocity dispersion of 0.4, and a flattening corresponding to that of an E4 galaxy, our remnant rotates like similarly flattened bright ellipticals (Illingworth 1981, 1983; Davies et al. 1983). Therefore, NGC 7252 probably will become an elliptical galaxy. It is then possible that other ellipticals (e.g., NGC 1587, as described in Borne & Hoessel 1988) were also produced through a similar disk-disk merger event of the sort presented here.

While our remnant rotates no more rapidly than do other ellipticals, the total angular momentum content of the system (including the unbound material stripped from the progenitor galaxies in the collision) is quite large. Schweizer (1982) points out that NGC 7252 is a relatively isolated galaxy, with no similar-brightness companion within ~ 1 Mpc h^{-1}. This is similar to the situation with NGC 1587 (Borne & Hoessel 1988), which is a *rapidly rotating* E1 galaxy in an *isolated* binary system, whose orbital angular momentum is nearly *parallel* to the spin of NGC 1587; the small companion galaxy NGC 1588 appears to contribute very little angular momentum to the system. Cosmological simulations that are used to support the traditional tidal torque theory should be examined to determine whether large net angular momenta can indeed be produced by tidal torques within such extensive low-density volumes of space as seen in these two cases.

It seems most unlikely to us that the main results of our study—that NGC 7252 is the result of a merger of two disks and that it will resemble an elliptical galaxy when virialized—are artifacts of the limitations of our technique. This view can be verified by using our "best-fit" model as a starting point in simulations with a "sticky" *N*-body code.

We wish to thank F. Schweizer for advice and encouragement, and for permitting us to reproduce his photograph of NGC 7252. For a critical reading of the manuscript and for many helpful suggestions, we thank A. Toomre and especially our referee J. Barnes. This research was supported in part by NSF grants 83-11414 and 87-20028 to the University of Michigan.

REFERENCES

Balcells, M., Borne, K. D., & Hoessel, J. G. 1989, *ApJ*, 336, 655
Barnes, J. E. 1988, ApJ, 331, 699
Bender, R. 1988, A&A, 202, L5
Borne, K. D. 1982, Ph.D. thesis, Caltech
———. 1984, ApJ, 287, 503 (Paper I)
———. 1988a, ApJ, 330, 38 (Paper II)
———. 1988b, ApJ, 330, 61 (Paper IV)
Borne, K. D., Balcells, M., & Hoessel, J. G. 1988, ApJ, 333, 567 (Paper V)
Borne, K. D., & Hoessel, J. G. 1988, ApJ, 330, 51
Borne, K. D., & Richstone, D. O. 1982, BAAS, 14, 972
Davies, R. L., Efstathiou, G., Fall, S. M., Illingworth, G., & Schechter, P. L. 1983, ApJ, 266, 41
Franx, M., & Illingworth, G. D. 1988, ApJ, 327, L55
Illingworth, G. 1981, in The Structure and Evolution of Normal Galaxies, ed. S. M. Fall & D. Lynden-Bell (Cambridge: Cambridge University Press), 27
———. 1983, in IAU Symposium 100, Internal Kinematics and Dynamics of Galaxies, ed. E. Athanassoula (Dordrecht: Reidel), 257
Jedrzejewski, R., & Schechter, P. L. 1988, ApJ, 330, L87
McGlynn, T. A., & Borne, K. D. 1990, ApJ, submitted
Schweizer, F. 1982, ApJ, 252, 455 (S82)
Toomre, A. 1977, in The Evolution of Galaxies and Stellar Populations, ed. B. M. Tinsley & R. B. Larson (New Haven: Yale University Observatory), 401
Toomre, A., & Toomre, J. 1972, ApJ, 178, 623 (TT)